

# Amphiphilic Polypeptoids Serve as the Connective Glue to Transform Liposomes into Multilamellar Structures with Closely Spaced Bilayers

Yueheng Zhang,<sup>†</sup> Sunting Xuan,<sup>‡</sup> Olasehinde Owoseni,<sup>†</sup> Marzhana Omarova,<sup>†</sup> Xin Li,<sup>§</sup> Michelle E. Saito,<sup>†</sup> Jibao He,<sup>||</sup> Gary L. McPherson,<sup>⊥</sup> Srinivasa R. Raghavan,<sup>#</sup> Donghui Zhang,<sup>\*,‡,§,||</sup> and Vijay T. John<sup>\*,†,||</sup>

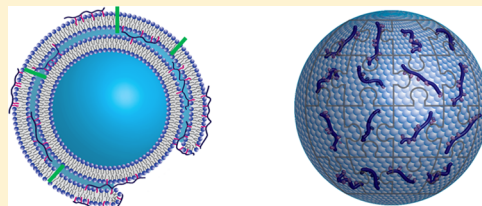
<sup>†</sup>Department of Chemical and Biomolecular Engineering, <sup>||</sup>Coordinated Instrumentation Facility, and <sup>⊥</sup>Department of Chemistry, Tulane University, New Orleans, Louisiana 70118, United States

<sup>‡</sup>Department of Chemistry and Macromolecular Studies Group and <sup>§</sup>Louisiana Consortium for Neutron Scattering, Louisiana State University, Baton Rouge, Louisiana 70803, United States

<sup>#</sup>Department of Chemical and Biomolecular Engineering, University of Maryland, College Park, Maryland 20742, United States

## S Supporting Information

**ABSTRACT:** We report the ability of hydrophobically modified polypeptoids (HMPs), which are amphiphilic pseudo-peptidic macromolecules, to connect across lipid bilayers and thus form layered structures on liposomes. The HMPs are obtained by attaching hydrophobic decyl groups at random points along the polypeptoid backbone. Although native polypeptoids (with no hydrophobes) have no effect on liposomal structure, the HMPs remodel the unilamellar liposomes into structures with comparable diameters but with multiple concentric bilayers. The transition from single-bilayer to multiple-bilayer structures is revealed by small-angle neutron scattering (SANS) and cryo-transmission electron microscopy (cryo-TEM). The spacing between bilayers is found to be relatively uniform at ~6.7 nm. We suggest that the amphiphilic nature of the HMPs explains the formation of multibilayered liposomes; i.e., the HMPs insert their hydrophobic tails into adjacent bilayers and thereby serve as the connective glue between bilayers. At higher HMP concentrations, the liposomes are entirely disrupted into much smaller micellelike structures through extensive hydrophobe insertion. Interestingly, these small structures can reattach to fresh unilamellar liposomes and self-assemble to form new two-bilayer liposomes. The two-bilayer liposomes in our study are reminiscent of two-bilayer organelles such as the nucleus in eukaryotic cells. The observations have significance in designing new nanoscale drug delivery carriers with multiple drugs on separate lipid bilayers and extending liposome circulation times with entirely biocompatible materials.



## INTRODUCTION

Liposomes are lipid-based vesicles that are of significant interest in drug delivery technologies because of their ability to encapsulate drug species and to be taken up by cells through fusion with cell membranes.<sup>1–5</sup> Ever since their discovery in 1965 by Bangham, who noticed the structural similarity to cell membranes, liposomes have been used in biophysical studies of phospholipid bilayers and as cell membrane mimics.<sup>6,7</sup> Newer applications of liposomes include their use as coatings on biomedical devices,<sup>8</sup> in single-molecule spectroscopy and biosensing,<sup>9,10</sup> and as submicrometer encapsulation systems in microfluidics.<sup>11</sup>

In many applications of liposomes, understanding the interaction of these vesicular systems with polymers becomes extremely important, whether to enhance circulation lifetimes, to control drug delivery rates, or to encapsulate liposomes in polymer matrixes. This article describes the interaction of liposomes with a class of synthetic molecules known as polypeptoids that are pseudo-peptidic materials with substituents attached to the nitrogen atoms of the polyglycine backbone.<sup>12,13</sup> These polymers have been of recent interest in chemical biology because of their highly designable structure

and their structural similarity to polypeptides.<sup>14,15</sup> Unlike polypeptides, however, polypeptoids lack extensive hydrogen bonding and backbone chirality because of their N-substitution, leading to a more flexible conformation and an enhanced resistance to proteolysis.<sup>16–18</sup> Because of backbone degradability, biocompatibility, and processability, polypeptoids are of promise in applications related to drug delivery carriers, tissue engineering materials, and smart coatings.<sup>19–21</sup> However, there is little information in the literature on polypeptoid interaction with lipids and cell membranes.

The objective of this study is to define and control the interactions of a model liposome system with two classes of polypeptoids in order to develop new concepts in liposome–polymer systems. The polymers chosen are (1) a polypeptoid containing the methoxyethyl (MeOEt) groups exclusively as side chains, hereafter denoted as an unmodified polypeptoid (UMP), and (2) a polypeptoid where about 26% of the MeOEt groups are randomly substituted by the *n*-decyl (C10) groups,

**Received:** November 23, 2016

**Revised:** February 14, 2017

**Published:** March 1, 2017

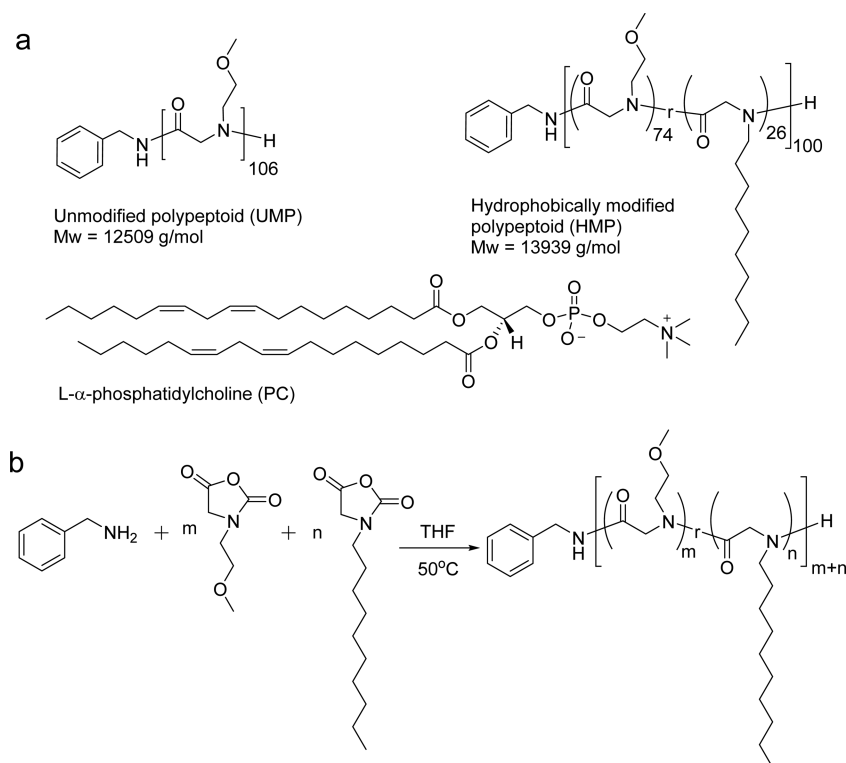


**Figure 1.** (a) Chemical structures of unmodified polypeptoid (UMP), hydrophobically modified polypeptoid (HMP), and  $L$ - $\alpha$ -phosphatidylcholine (PC). (b) Synthesis route to the polypeptoids.

hereafter denoted as a hydrophobically modified polypeptoid (HMP) as shown in Figure 1a. Both polypeptoids can be synthesized through the route shown in Figure 1b.

The presence of the hydrophobic alkyl groups leads to the attachment of polymers to the lipid bilayers through the insertion of alkyl groups into the bilayer as a consequence of hydrophobic interaction. Such insertions of hydrophobic groups into the bilayer are inherent properties of polymeric surfactants (polysoaps),<sup>22,23</sup> peptide amphiphiles,<sup>24</sup> and lipopolypeptoids.<sup>25</sup> In the case of a lipid-conjugated poly(ethylene glycol) (PEG) (such as 1,2-distearoyl-*sn*-glycero-3-phosphoethanolamine-*N*-amino(polyethylene glycol), DSPE-PEG), the polymer chain is attached to the liposome surface through insertion of the hydrophobic distearoyl group into the lipid bilayer.<sup>26</sup> This is important for extending the circulation times of liposomes for drug delivery. Bis-alkyl hydrophobes attached to PEG have been shown by Auguste and co-workers to bind more strongly to the bilayer in comparison to monoalkyl hydrophobes.<sup>27</sup> Work by Shen and co-workers have shown the potential for bis-alkyl lipopolymers to tether lipid bilayers to surfaces.<sup>28</sup> When a small fraction (<5%) of alkyl groups are present on long-chain polymers such as hydrophobically modified chitosan (hm-chitosan), the liposomes are connected into a network by the polymer chains.<sup>29</sup> Hydrophobic interactions are intrinsic in understanding the effects of surfactants on lipid bilayers, where liposomes and cell membranes have been found to break down through fluidization of the bilayer and eventual dissolution of the lipids into mixed lipid-surfactant micelles.<sup>30–33</sup>

We have found several unique and distinct features in the interactions of HMPs with liposomes, which we elaborate on in this article. Specifically, HMPs seem to stitch together vesicle bilayers, leading to multilayered liposomes with small and

relatively uniform spacings between their concentric bilayers. Such structures have not been observed before. The formation of these multilayered structures is confirmed by a combination of SANS and cryo-TEM.

## EXPERIMENTAL SECTION

**Materials.**  $L$ - $\alpha$ -Phosphatidylcholine (PC) was purchased from Avanti Polar Lipids. Deuterium oxide was purchased from Cambridge Isotope Laboratories. Deionized (DI) water generated by an ELGA reverse osmosis water purification system (MEDICA 15BP) with a resistance of 18.2 M $\Omega$ -cm was used in all experiments. All chemicals were used as received unless otherwise noted.  $N$ -Decyl  $N$ -carboxyanhydride ( $N$ -decyl NCA) in 53–57% yield and  $N$ -methoxyethyl  $N$ -carboxyanhydride ( $N$ -methoxyethyl NCA) in 43–49% yield were synthesized by adapting previously reported procedures, as shown in Supporting Information Figure S1 (routes I and II).<sup>34,35</sup>

**Synthesis of Polypeptoids.** The polypeptoids were synthesized in a glovebox through benzyl amine-initiated ring-opening polymerization of the corresponding  $N$ -substituted  $N$ -carboxyanhydride (R-NCA) monomers. The unmodified polypeptoid (UMP), poly( $N$ -methoxyethyl glycine) (PNMeOEtG), was synthesized by the polymerization of  $N$ -methoxyethyl NCA, whereas the hydrophobically modified polypeptoid (HMP), poly[ $N$ -methoxyethyl glycine-*r*-( $N$ -decyl glycine)] (P(NMeOEtG-*r*-NDG)), was synthesized by the copolymerization of  $N$ -methoxyethyl NCA and  $N$ -decyl NCA (Figure 1b). Both UMP and HMP are designed to reach a polymerization degree of 100. In a typical synthesis of HMP, stock solutions of  $N$ -methoxyethyl NCA (1.3 mL, 0.4 M, 0.52 mmol) and  $N$ -decyl NCA (0.3 mL, 0.4 M, 0.13 mmol) in THF were mixed in a small vial. Benzyl-NH<sub>2</sub>/THF stock solution (70  $\mu$ L, 92.7 mM, 6.5  $\mu$ mol) was added to the above mixture and held at 50 °C for 48 h. Aliquots were taken and analyzed by <sup>1</sup>H NMR spectroscopy to check the conversion. The polymer was precipitated out by adding excess hexane, collected by filtration, and dried under vacuum to obtain the final product as a white solid (61.6 mg, 88.2% yield).

**NMR and Size-Exclusion Chromatography (SEC) Analysis of the Polypeptoids.**  $^1\text{H}$  and  $^{13}\text{C}\{^1\text{H}\}$  NMR spectra were obtained by using a Bruker AV-400 Nanobay spectrometer (400 MHz for  $^1\text{H}$  NMR and 100 MHz for  $^{13}\text{C}\{^1\text{H}\}$  NMR) at 298 K. Chemical shifts ( $\delta$ ) given in parts per million (ppm) were referenced to proton impurities or the  $^{13}\text{C}$  isotopes of deuterated solvents ( $\text{CDCl}_3$ ,  $\text{CD}_2\text{Cl}_2$ , and  $\text{D}_2\text{O}$ ).  $^1\text{H}$  NMR (Supporting Information Figure S2) and  $^{13}\text{C}\{^1\text{H}\}$  NMR (Supporting Information Figure S3) of the monomers are included in the Supporting Information. SEC analysis of the polypeptoids was performed by using an Agilent 1200 system (Agilent 1200 series degasser, isocratic pump, autosampler, and column heater) equipped with three Phenomenex  $5\ \mu\text{m}$ ,  $300 \times 7.8\ \text{mm}^2$  columns [ $100\ \text{\AA}$ ,  $1000\ \text{\AA}$ , and Linear (2)], a Wyatt OptilabEX differential refractive index (DRI) detector with a 690 nm light source, and a Wyatt DAWN EOS multiangle light scattering (MALS) detector (GaAs 30 mW laser at  $\lambda = 690\ \text{nm}$ ). DMF with 0.1 M LiBr was used as the eluent at a flow rate of  $0.5\ \text{mL}\cdot\text{min}^{-1}$ . The column and detector temperature was set at  $25\ ^\circ\text{C}$ . All data analysis was performed using Wyatt Astra V 5.3 software. The polydispersity index (PDI) was obtained by conventional SEC analysis with a calibration curve. The calibration curve was constructed from 23 pauci-disperse polystyrene standards ( $M_n = 590\ \text{g}\cdot\text{mol}^{-1}$ – $1472\ \text{kg}\cdot\text{mol}^{-1}$ , Polymer Laboratories, Inc.) using Astra's column calibration template. The relative PDI was then calculated by using Astra's conventional calibration template. The sample for SEC analysis was prepared as below:  $130\ \mu\text{L}$  of the reaction mixture of HMP (or UMP) was added to 1 mL of DMF with 0.1 M LiBr and mixed thoroughly. This mixture was directly injected into the SEC instrument for analysis.

**Liposome Preparation.**  $1\text{-}\alpha$ -Phosphatidylcholine (PC) liposomes were prepared by using the thin film hydration method.<sup>36</sup> PC (0.1 g) was first dissolved in a round-bottomed flask by 15 mL of a mixed solution of chloroform and methanol in a volume ratio of 2:1. The solvent was then evaporated using a rotary evaporator (Buchi R-205) at room temperature under 100 mbar for 3 h to form a thin lipid film. The pressure was further reduced to 6 mbar for 30 min to remove residual solvent. The obtained thin lipid film was hydrated with DI water at  $50\ ^\circ\text{C}$ . The aqueous suspension was transferred to a syringe and extruded 21 times through a 100 nm polycarbonate membrane to acquire liposomes with an average diameter of 100 nm.

**Preparation of Liposome and Polypeptoid Mixtures.** DI water was used to dilute the liposome stock suspension to 0.5%. HMP solutions at concentrations of 0.25, 0.5, 0.75, and 1% were mixed with a 0.5% liposome suspension in a 1:1 volume ratio to acquire solutions with the liposome concentration fixed at 0.25% and varying concentrations of HMP. The resulting mixtures were labeled as LIP0125HMP, LIP025HMP, LIP0375HMP, and LIP05HMP, denoting the final overall concentrations of HMP. Liposomes were also incubated with UMP at overall concentrations of 0.25 and 0.5% as negative controls, denoted as LIP025UMP and LIP05UMP, respectively. The liposome solution with an overall concentration of 0.25% was used as the blank control, denoted as LIP. Essentially all of the samples had the same concentration of lipid (0.25%), and the studies were done with varying concentrations of polymers. All samples were incubated for at least 12 h prior to instrumental characterization. All concentrations are reported as wt %.

**SANS Data Collection and Reduction.** The SANS experiments were carried out on the extended-Q-range small-angle neutron scattering (EQ-SANS) diffractometer at the Spallation Neutron Source (SNS) at Oak Ridge National Laboratory (ORNL). All samples were prepared with pure deuterium oxide to generate sufficient scattering contrast. The samples were loaded into 2-mm-path-length quartz banjo cells (Hellma, Germany) and placed in a 42-position sample chamber. Measurements were made at room temperature ( $20\ ^\circ\text{C}$ ). The instrument was operated in 60 Hz mode with a neutron wavelength ( $\lambda$ ) range of 2.5–6.1  $\text{\AA}$ . The sample-to-detector distance was set to 4 m. This configuration provides an effective  $q$  range of  $0.009$ – $0.44\ \text{\AA}^{-1}$ . The scattering vector,  $q$ , is defined by  $q = 4\pi[\sin(\theta/2)]/\lambda$ , where  $\theta$  is the scattering angle.

The reduction of SANS data was performed using MantidPlot software following standard procedures.<sup>37</sup> The data were corrected for

instrument dark current, detector sensitivity, incident beam normalization, sample transmission, and solvent background. A calibrated standard provided by ORNL, Porasil B, was used to obtain the scale factor that was used to convert the data into absolute intensity units ( $\text{cm}^{-1}$ ). Reduced data were azimuthally averaged using MantidPlot to generate the scattering intensity per unit volume,  $I(q)$ , as a function of  $q$ .

**Cryo-TEM Imaging.** Cryo-TEM imaging was done on an FEI G2 F30 Tecnai TEM operated at 150 kV. To prepare the sample, a 300-mesh lacey carbon grid (Electron Microscopy Sciences) was picked up with tweezers and mounted on the plunging station of an FEI Vitrobot. Ten microliters of the solution was applied to the grid. The excess liquid was blotted by filter paper attached to arms of the Vitrobot for 2 s to form a thin film. The sample was then vitrified by plunging into liquid ethane. The vitrified sample was finally transferred onto a single-tilt cryo specimen holder for imaging.

## RESULTS AND DISCUSSION

**Polypeptoid Characterization through  $^1\text{H}$  NMR and Size-Exclusion Chromatography (SEC).** The compositions of UMP and HMP were determined by  $^1\text{H}$  NMR spectroscopy (Supporting Information Figure S4). The number-average degree of polymerization (DP) of UMP was determined by the integration of the methylene group in the backbone at 4.52, 4.41, 4.18, and 4.10 ppm relative to the integration of the benzyl end-group at 7.24 and 7.31 ppm. The DP of HMP was determined by the integration of the methyl group into the side chain and the integration of methylene groups into the backbone relative to the integration of the benzyl end-group at 7.24 and 7.31 ppm. The integrations give UMP a DP of 106 and HMP a DP of 100 containing 26 mol % *N*-decyl glycine units, corresponding to molecular weight of 12 509 g/mol for UMP and 13 939 g/mol for HMP. The size-exclusion chromatography (SEC) analysis indicated the monomodal and narrow distributions of polymer molecular weight for both UMP and HMP (Supporting Information Figure S5), with low PDIs of 1.09 and 1.08, respectively.

**Small-Angle Neutron Scattering (SANS).** As the first step in the characterization of the interactions between the polymers and liposomes, we carried out SANS experiments on the individual systems with the results shown in Figure 2. As shown here, the data are separated by a scale factor of 0.1 for clarity and ease of visualization especially at the larger  $q$  values. The scattering intensity,  $I(q)$ , is determined by the structure factor,  $S(q)$ , and the form factor,  $P(q)$ . In a dilute, noninteracting system,  $S(q)$  is close to 1. Therefore,  $I(q)$  is determined by  $P(q)$ .<sup>38</sup>

Curve a in Figure 2 shows the scattering profile of a 0.25% liposome suspension (LIP). For a detailed analysis of the form factor, the scattering data was fitted to the PolyCoreMultiShell model developed by the National Institute of Standards and Technology (NIST) using IgorPro software. When  $N$  (model parameter, number of shells) is fixed at 1,  $P(q)$  can be described as<sup>39,40</sup>

$$P(q) = \frac{\text{scale}}{V_{\text{shell}}} \left[ \frac{3V_1(\rho_1 - \rho_2) J_1(qR_1)}{qR_1} + \frac{3V_2(\rho_2 - \rho_{\text{solv}}) J_1(qR_2)}{qR_2} \right]^2 + \text{bkg} \quad (1)$$

where scale is a scale factor,<sup>39</sup>  $V_{\text{shell}}$  is the volume of the shell,  $V_1$  is the volume of the core,  $V_2$  is the total volume,  $R_1$  is the radius of the core,  $R_2$  is the outer radius of the shell,  $\rho_1$  is the scattering-length density of the core,  $\rho_2$  is the scattering-length density of the shell,  $\rho_{\text{solv}}$  is the scattering-length density of the solvent, bkg is the background level, and  $J_1(x) = (\sin x - x \cos$

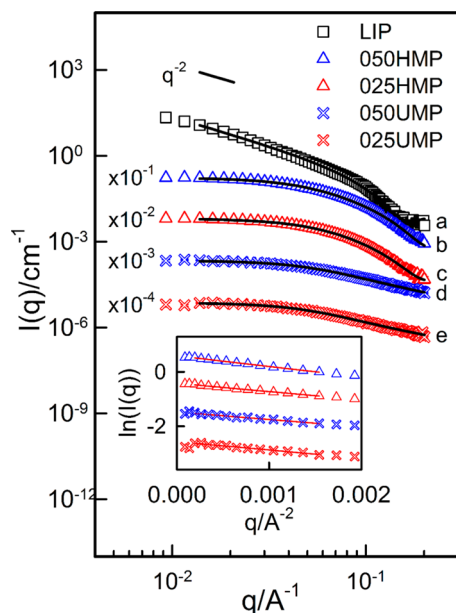


**Figure 2.** Scattering profiles of 0.25% liposome (LIP, a), 0.5% HMP (050HMP, b), 0.25% HMP (025HMP, c), 0.5% UMP (050UMP, d), and 0.25% UMP (025UMP, e) in D<sub>2</sub>O. The curves are scaled and separated by a factor of 0.1. The solid lines are best-fit results to the corresponding models. The inset shows the Guinier plots ( $\ln(I)$  vs  $q^2$ ) of the HMP and UMP samples.

$x)/x^2$ . With polydispersity in the core radius being considered, the form factor is averaged over the Schultz distribution<sup>38</sup>

$$P(q) = \int f(R) P(q, R) dR \quad (2)$$

$$f(R) = \left( \frac{z+1}{R_0} \right)^{z+1} \frac{R^z}{\Gamma(z+1)} \exp \left[ -(z+1) \frac{R}{R_0} \right] \quad (3)$$

where  $f$  is the distribution function,  $R$  is the core radius,  $R_0$  is the average core radius,  $\Gamma(x)$  is the gamma function, and  $z$  is the polydispersity index. The polydispersity,  $p$ , is related to  $z$  through

$$p = \frac{1}{\sqrt{z+1}} \quad (4)$$

The scattering profile of the liposome system (Figure 2, curve a) indicates a  $q^{-2}$  dependence in the decay in the low  $q$  range, which is characteristic of noninteracting liposomes.<sup>32</sup> The solid line shows the best fit of the scattering data of liposomes. The fitting results show a liposome diameter of 99.4 nm with a polydispersity of 0.17. The shell thickness, or the lipid bilayer thickness, is 3.68 nm, which is close to the reported value in the literature.<sup>41,42</sup>

**Table 1.** Model Fitting Parameters for SANS Data

sample	components	$R_{\text{cyl}}$ (nm) <sup>a</sup>	$L$ (nm) <sup>b</sup>	$b$ (nm) <sup>c</sup>	$R_g$ (nm) <sup>d</sup>
025HMP	0.25% HMP	1.7	38.0	0.76	3.0
050HMP	0.5% HMP	1.7	38.0	1.08	3.4
025UMP	0.25%UMP	0.6	39.4	1.00	3.0
050UMP	0.5% UMP	0.6	39.4	0.87	2.9
LIP050HMP	0.25% liposome 0.5% HMP	2.0	38.0	3.43	4.7

<sup>a</sup> $R_{\text{cyl}}$ : cylinder radius. <sup>b</sup> $L$ : contour length. <sup>c</sup> $b$ : Kuhn length. <sup>d</sup> $R_g$  values are acquired from Guinier analysis.

We found that the scattering curves for HMP samples were best fitted to the flexible cylinder model.<sup>43,44</sup> For UMP, the curve was also fitted by the Gaussian coil model, but we retained the excellent fit of the flexible cylinder model to provide a direct comparison of parameters with HMP. In both cases, we assumed that the contour length  $L$  was much greater than the Kuhn length  $b$ . The results are presented in Figure 2 as solid black lines.  $L$  was calculated on the basis of the degree of polymerization and was fixed in the flexible cylinder model calculations to estimate  $b$  and the axial radius of the polymer aggregates,  $R_{\text{cyl}}$ . The radius of gyration,  $R_g$ , of each sample was also calculated from the model fit results.<sup>43</sup> The results are included in Table 1.

The inset in Figure 2 shows the empirical Guinier plots where data in the range of  $0.00014 \text{ \AA}^{-2} < q^2 < 0.0016 \text{ \AA}^{-2}$  were used in the calculation of  $R_g$ . The results of the Guinier analysis are listed in Table 1 and show very reasonable agreement with the  $R_g$  values calculated from the model fitting results. To summarize Table 1, the values of  $R_g$  between UMP and HMP show insignificant differences at both concentrations, and we infer that the state of the polymers over this range of concentration remains essentially the same. The fact that the form factor fits the low  $q$  range in these dilute systems may additionally imply that there is minimal intermolecular aggregation. As shown in the subsequent discussion, significant changes in  $R_g$  values are obtained through the interaction of HMP with lipid bilayers.

To explore the interactions between liposomes and polypeptoids, we prepared solutions containing 0.25% liposomes with 0.25 and 0.5% UMP as control samples. The SANS data for these samples (LIP025UMP and LIP050UMP, respectively) are shown in Figure 3. At low  $q$ , the slope of the

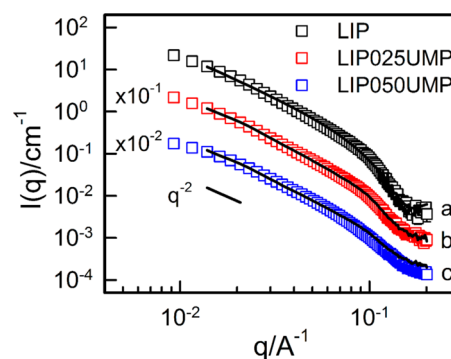


**Figure 3.** Scattering profiles of 0.25% liposomes incubated with 0% UMP (LIP, a), 0.25% UMP (LIP025UMP, b), and 0.5% UMP (LIP050UMP, c). The scattering curves are separated by a scale factor of 0.1 for clarity. The addition of UMP has little effect on the scattering pattern, which is essentially a linear summation of the scattering data of the individual components.

scattering curve remains  $-2$  when liposomes are mixed with UMPs, which is indicative that the bilayer structure is maintained when the liposome is incubated with UMPs. We note that the scattering intensity of the mixtures is essentially just the concentration-weighted summation of the individual components with the scattering from the liposomes dominating the pattern at low  $q$ . These observations indicate that there is no structural change in the system induced by UMP and that UMP and liposomes exist as independent entities in solution.

Figure 4 illustrates the scattering patterns of mixtures of liposomes and HMP, and it is immediately clear that there are

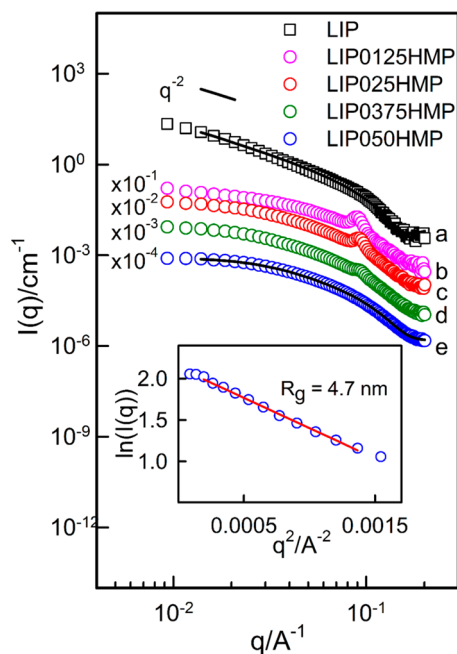


**Figure 4.** SANS data of 0.25% liposomes incubated with 0% HMP (LIP, a), 0.125% HMP (LIP0125HMP, b), 0.25% HMP (LIP025HMP, c), 0.375% HMP (LIP0375HMP, d), and 0.5% HMP (LIP050HMP, e). The scattering curves are separated by a scale factor of 0.1 for clarity. The black solid lines show best-fit results to the corresponding models. The inset shows the Guinier plot of the scattering data of LIP0125HMP, giving an  $R_g$  of 4.7 nm.

significant changes in the patterns in comparison to the scattering from LIP. With the addition of HMP, the slope of the scattering curve in the low  $q$  range flattens significantly, indicating changes in the liposome bilayer structure. Along with this, a significantly decreased intensity in the low  $q$  range was observed for each sample with HMP added compared to the control sample. (Supporting Information Figure S6 shows the unscaled data for the plots in Figure 4.) We additionally see a Bragg diffraction peak at around  $q = 0.092 \text{ \AA}^{-1}$  at an HMP concentration of 0.125%, which shifts to slightly higher  $q$  and decreases in intensity with increased addition of HMP. The drop in scattering intensity at low  $q$  with the addition of more scattering entities (HMPs) and the observation of the Bragg peak are counterintuitive and are not easily fit using models for neutron scattering profiles. The drop in scattering intensity points to a decrease in the number density of the larger scattering entities (liposomes), and the Bragg peak suggests the occurrence of layered structures with relatively uniform spacing. But to better understand these SANS observations, we have used cryo-TEM, and the imaging results for all samples used in SANS analysis are described below.

**Cryo-Transmission Electron Microscopy of Microstructures.** Figure 5a and b show cryo-TEM images of the control samples containing liposomes alone (Figure 5a) and liposomes incubated with UMP (Figure 5b), where we have done higher-resolution imaging to verify the unilamellarity of the liposomes. The clear observations are that the unilamellar PC liposomes are unchanged by the addition of UMP, in agreement with the SANS results. It is therefore evident that the liposomes are stable in the presence of UMPs and that liposome–UMP interactions do not affect the liposome structure.

Figure 5c–e illustrates the cryo-TEM images of liposomes incubated with varying concentrations of HMP. With 0.125% HMP addition, although there is no significant change in the size of liposomes, there is the interesting visualization of a second lipid layer, with the higher-resolution image of Figure 6c showing that the layer is incomplete. We also observe liposomes with multiple bilayers (inset to Figure 5c). With cryo-TEM, it is not possible to determine the number density of imaged objects because the number density varies at different locations on the grid. Nevertheless, we observed a reduced density of liposomes over the TEM field of view. The

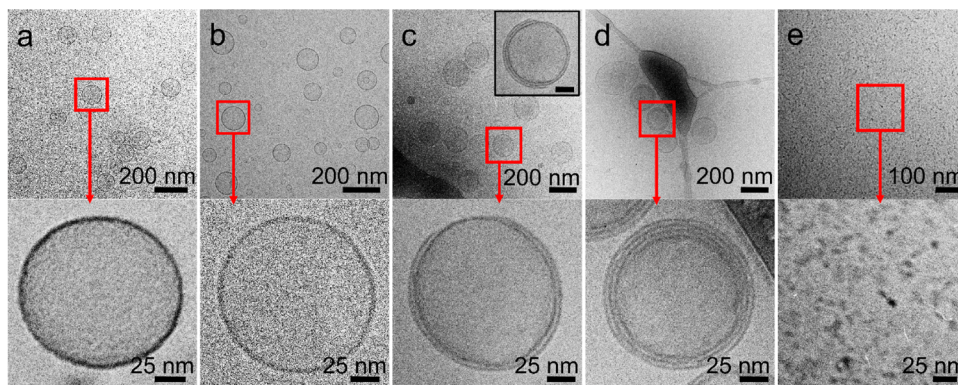


**Figure 5.** Cryo-TEM images of 0.25% liposome incubated in DI water (LIP, a), 0.25% UMP (LIP025UMP, b), 0.125% HMP (LIP0125HMP, c), 0.25% HMP (LIP025HMP, d), and 0.5% HMP (LIP050HMP, e) and corresponding high-magnification images below them (red square). Although the addition of UMP has no effect on the liposome structure, the addition of HMP to the liposome suspension results in a transition from unilamellar structure to two-bilayer (c) and multiple-bilayer (d) structures and finally a solubilization of liposome (e). The inset in c indicates that liposomes with multiple layer structures also exist in the LIP0125HMP sample but with a small population. The scale bar of the inset is 50 nm.

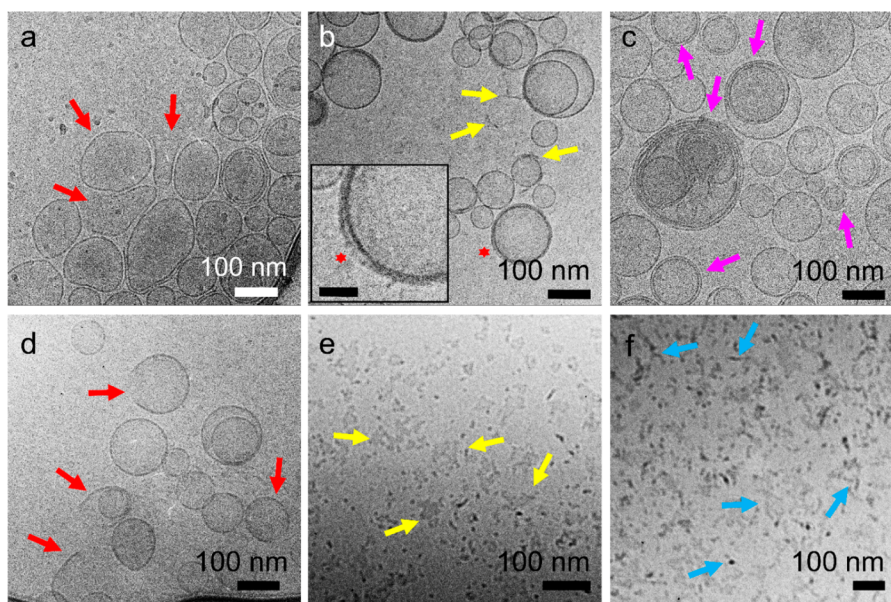


**Figure 6.** (a–c) Cryo-TEM images of 0.25% liposomes incubated with 0.25% HMP (LIP025HMP) for 1 (a), 20 (b), and 45 min (c). In a, arrows show deformed liposomes and open bilayer structures; in b, arrows show fragments of liposomes and the inset shows the two bilayers of the started liposome (scale bar 50 nm); and in c, arrows show liposomes with multilayered structures. (d–f) Cryo-TEM images of 0.25% liposomes incubated with 0.5% HMP (LIP050HMP) for 1 (d), 20 (e), and 45 min (f). Arrows in d show open bilayer structures; arrows in e show small fragments and the sample has no remnant intact liposomes; and in f, small nanoscale structures are observed (typical structures are pointed to by the arrows).

observation of a reduced number density becomes more pronounced with the addition of HMP to a concentration of 0.25%, and again we see the presence of liposomes with multiple bilayers (Figures 5d). In all of these cases, the number of bilayers varies, and the formed additional layers are not necessarily complete and uniform. The average distance between each two adjacent layers (center-to-center distance) in the high-magnification image of Figure 5d was measured using Nano Measure software. Multiple measurements were taken at different locations, and the results were averaged. The measured average spacing distance is  $6.8 \pm 0.9$  nm, which agrees very well with the observed Bragg peak at a  $q$  value of  $0.092 \text{ \AA}^{-1}$  corresponding to a  $d$  spacing of 6.8 nm. To our knowledge, this is the first observation of liposomes with two or more bilayers with a relatively uniform spacing of a few nanometers.

When the HMP concentration is further increased to 0.5%, the SANS data shows the loss of the Bragg peak (curve e in Figure 4). On the cryo-TEM, we are unable to see any liposomes in the TEM field of view, indicating a complete disassembly of liposomes. However, we see clear evidence of small nanoscale structures (Figure 5e). A close examination of the images reveals that some of the shapes in the 2-D image appear somewhat circular with dimensions of around 5 nm and some appear elongated as small wormlike structures with a 5 nm thickness and a length of 10–15 nm. The circular dots typically have a higher contrast, perhaps indicative of a coiled globular structure or of rods vitrified with axes parallel to the beam. The scattering curve at this HMP concentration can be again modeled through the flexible cylinder model (Table 1). The  $R_g$  value calculated from the model fitting result is 5.1 nm and the Guinier plot (inset to Figure 4) shows the  $R_g$  value of 4.7 nm, and we note that these values are much smaller than liposomal dimensions but appreciably larger than the values for UMP and HMP alone. These suggest that the liposomes are converted to such new nanoscale structures upon addition of

HMPs. We also note that HMP, when added to the hydrating solution at 0.5 wt %, prevents the formation of the large liposomes typically observed prior to extrusion and leads to the formation of small fragments similar to Figure 5e. The formation of liposomes is also inhibited when HMP is integrated into the lipid film prior to the hydration step. Supporting Information S7 provides a cryo-TEM image of the small fragments formed when HMP is integrated into the lipid film and then hydrated. These observations indicate the generality of the phenomenon of liposome disruption by HMP.

Both SANS and cryo-TEM reveal the important observation that HMP disrupts liposomes and at sufficiently high concentrations completely disassembles these vesicular structures. But most importantly, it is an additional conclusion that at intermediate concentrations the HMPs induce the liposomes to fuse, which leads to the creation of two or more bilayer structures on surviving liposomes. We propose that it is the formation of such multilayer liposomes that gives rise to the Bragg peak in the scattering.

Although the above results relate to equilibrated samples, cryo-TEM makes it possible to gain an understanding of the dynamics of the structural transformations by contacting the liposomes with HMP and rapidly vitrifying the systems at varying incubation times. Thus, 0.25% liposome was incubated with 0.25% HMP (LIP025HMP) for 1, 20, and 45 min, after which they were vitrified for cryo-TEM imaging. The sample incubated for 1 min (Figure 6a) shows a significant deformation of liposomes and open bilayer structures. After 20 min (Figure 6b), we see evidence of the formation of two bilayer structures and liposome rearrangement. At this stage, while the liposomes are multilayered, the spacing between bilayers is not uniform and is considerably larger than the equilibrium value. At 45 min, liposomes with a multilayered structure are observed (Figure 6c), with bilayer spacing down to  $\sim 7$  nm. This result suggests that the formation of multilayer liposomes undergoes a stepwise process. After HMP is

incorporated into the bilayers, liposomes first partially break up and form open bilayer structures or large sheets (incomplete liposomes). The incomplete liposomes attach to surviving liposomes through hydrophobe insertion into bilayers to form multilayer structures. HMP thus serves as a connective material between the liposome bilayer and additional bilayers. This is distinctly different from small-molecule surfactants (with a single hydrophobic tail) that simply fluidize and eventually break up liposomes into mixed micelles of surfactant and lipid.<sup>24,27</sup>

Figure 6d–f illustrates the identical experiments but with 0.5% HMP (LIP050HMP). Within 1 min of mixing, broken liposomes with open structures are observed (Figure 6d). After 20 min of incubation, we see the coexistence of small fragments and debris (Figure 6e). With 45 min of incubation (Figure 6f), a complete breakdown of the liposomes occurs with the same suspended nanoscale structures as observed in Figure 5e.

On the basis of the SANS and cryo-TEM observations, we propose the following mechanism for the results of liposome–HMP interactions as shown in Figure 7. At the lower HP

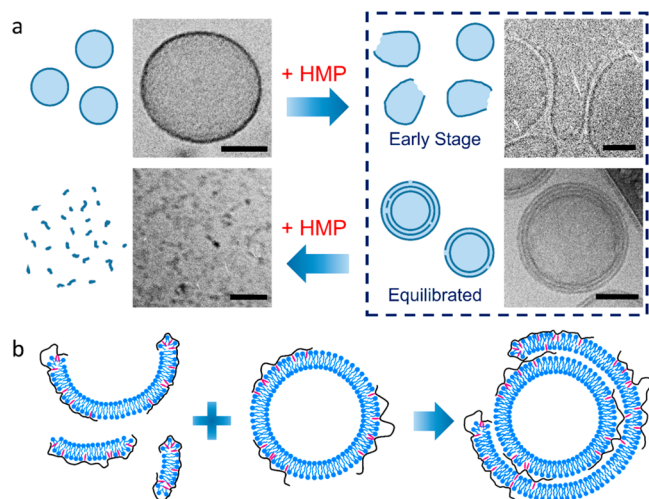


**Figure 7.** (a) Schematic of the formation of multiple-bilayer liposomes and the solubilization of liposomes induced by HMP. (The scale bars in all images are 50 nm.) (b) Illustration of HMP bridging the fragments and lipid bilayer of a liposome by hydrophobe insertion forming a two-bilayer structure.

concentrations, a fraction of the liposomes is broken into large fragments by the insertion of hydrophobes that have a sufficient local concentration in the bilayer to fluidize and disrupt the bilayer. Such softening of lipid bilayers through hydrophobe insertion is considered the dominant mechanism of liposome disruption by detergents. Thus, with detergents at low concentrations, bilayer fluidity is increased by the insertion of the low-molecular-weight surfactant tails. After a critical level of detergent addition, the bilayer loses its mechanical integrity, and liposomes become disrupted into mixed lipid–detergent micelles.<sup>35–38</sup> Polymeric hydrophobe-containing amphiphiles such as HMPs are distinct because the local concentration of hydrophobes inserted into lipid bilayers determines the fate of the bilayer. With the highly substituted HMP used in these experiments, there clearly is a sufficient local concentration of hydrophobes to locally fluidize and break liposomes. At low HMP concentrations, not all liposomes become exposed to the polymer, and those exposed to the polymer become disrupted

into large fragments because fluidization occurs only at specific segments of the liposome bilayer. At higher HMP concentrations, all liposomes become exposed to the polymer and break into small fragments because fluidization occurs at multiple points of the liposomal bilayer.

But the key observation of using such polymer-based amphiphiles appears to be the ability to bridge between lipid bilayers. We postulate that in the lipid + HMP complex there are always a few free contacts (hydrophobes that transiently become free rather than inserted into the lipid bilayer) that are sufficient to conduct interlayer bridging. Thus, at the lower HMP concentrations, fragments with attached HMPs can reattach to remnant intact liposomes either through the insertion of some of the free hydrophobes into the bilayer of intact liposomes or through interaction with other HMP chains that may be attached to the unbroken liposome (Figure 7b). We propose that the attachment of these fragments may continue to the formation of multiple layers and the spacings are sufficiently periodic to give rise to the constructive interference in neutron diffraction leading to the observed peak at a  $d$  spacing of 6.8 nm. The formation of multilayered structures is thus a stepwise process. Initially, some of the liposomes are broken into fragments while other liposomes remain intact. Then the fragments attach to the surfaces of intact liposomes to form additional layers. At high HMP concentrations, the incorporation of additional HMPs into lipid bilayers results in a solubilization of lipid bilayers by forming lipid–HMP small elongated structures that are modeled by flexible cylinders.

The hypothesis that fragments with the hydrophobes containing polymer can be hooked onto lipid bilayers was tested through the reverse experiment of contacting the completely broken down liposome system as shown in Figure 5e with a suspension of fresh intact liposomes. The experiment was carried out by mixing the LIP050HMP solution with a fresh batch of liposomes (LIP) in a volume ratio of 1:2 (Figure 8a). Remarkably, incomplete layers form on the surface of the new liposome, and it is difficult to visualize any remaining broken up structures (Figure 8b). The two-bilayer structure is therefore reconstructed. The continuity of the second layer implies the possibility of surface diffusion of the fragments that first attach to the intact liposomes and that upon contact, connect to each other through hydrophobe insertion (Figure 8c). Our proposed explanation of this observation is again that the dynamic nature of the hydrophobes allows a few of them in the lipid–HMP complex to be exposed, thus allowing the insertion into the bilayer of intact liposomes. The concentration of exposed hydrophobes is insufficient to disrupt intact liposomes.

## CONCLUSIONS

In this study, we have demonstrated that the introduction of decyl groups into a hydrophilic polypeptoid backbone can induce interactions between the modified polypeptoid and liposomes through the insertion of hydrophobes into the lipid bilayer. This leads to a breakdown of the liposome structural integrity and a gradual solubilization of the liposome into mixed aggregates of lipids and the modified polypeptoid. In this respect, the phenomenon is similar to the interaction of small-molecule surfactants with liposomes. A distinct difference, however, is the ability of the HMP polymeric amphiphile to attach fragments onto existing and surviving liposomes to create additional layers on the surface of liposomes. The

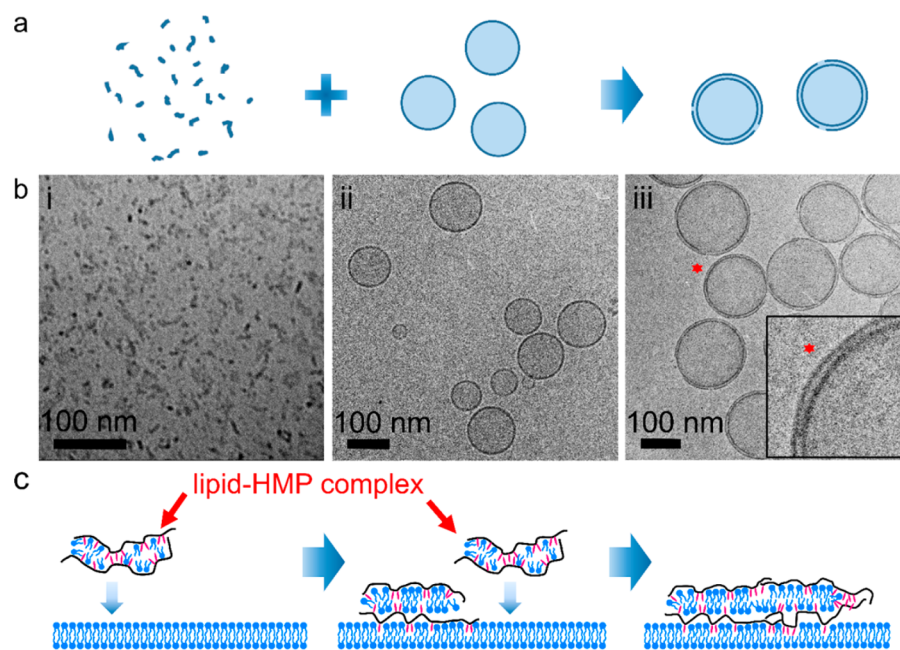


**Figure 8.** (a) Schematic of the experiment showing the addition of a lipid–HMP complex solution (LIP050HMP) to a fresh liposome suspension (LIP) in a volume ratio of 1:2. (b) Cryo-TEM images show the lipid–HMP complex (i), fresh liposome (ii), and reconstructed bilayers on bare liposomes (iii). The inset in iii shows the reconstructed bilayer on the liposome (identified by the asterisk with scale bar 25 nm). (c) Schematic of building up a bilayer structure from lipid–HMP complexes. When the lipid–HMP complexes contact bare liposomes, HMP incorporates into the bilayers by hydrophobe insertion into the fresh bilayers. The assembly of such attachment results in the formation of additional lipid bilayers.

polymer chain serves as the connecting material between lipid-containing fragments and liposomal bilayers, allowing a buildup of bilayers on the surface of a liposome. In contrast to small-molecule surfactants, such polymeric surfactants have membrane interaction properties that may be adjusted both through the polymer concentration and the relative degree of hydrophobe substitution on the chain backbone. The concepts we have shown should be completely general, and other interfacially active polymers with a high degree of alkyl substitution may indeed break liposomes. These are aspects of our continuing detailed studies with polypeptoids where we change the degree of substitution and the molecular weight. The intrinsic biocompatibility of polypeptoids and the fact that their sequence and functional groups can be designed are appealing aspects of conducting further research to understand their properties with respect to lipid bilayers and cell membranes.

The potential to build bilayers onto liposomes using a designed connective polymeric amphiphile has significant technical implications. These concepts may have relevance in the attachment of drug-containing lipid entities to cell membranes and to vesicle systems. The ability of HMPs to remodel liposomes is a novel aspect of multilayer self-assembly with significant applications to using liposomes as multiple drug carriers. For example, it may be possible to load the interior of the liposome with water-soluble drugs and the bilayer with a hydrophobic drug. Subsequently, the patchwork addition of a second bilayer containing additional drug or diagnostic components may lead to multilamellar liposomes with multiple therapeutics or sensing agents. We also note that the double-bilayer structure has a resemblance to those found in organelles such as in the nuclear membrane of eukaryotic cells, although the bilayer spacing here is smaller. Our continuing research seeks to understand these effects in realizing new applications.

## ■ ASSOCIATED CONTENT

### 📄 Supporting Information

The Supporting Information is available free of charge on the ACS Publications website at DOI: [10.1021/acs.langmuir.6b04190](https://doi.org/10.1021/acs.langmuir.6b04190).

Synthesis of monomers,  $^1\text{H}$  NMR of monomers and polypeptoids,  $^{13}\text{C}\{^1\text{H}\}$  NMR of monomers, SEC chromatograms of polypeptoids, unscaled SANS profiles of polypeptoids and lipid mixtures at low  $q$ , and cryo-TEM image of lipid-HMP thin films (PDF)

## ■ AUTHOR INFORMATION

### Corresponding Authors

\*(D.Z.) Phone: 225-578-4893. E-mail: [dhzhang@lsu.edu](mailto:dhzhang@lsu.edu).  
\*(V.T.J.) Phone: 504-865-5883. E-mail: [vj@tulane.edu](mailto:vj@tulane.edu).

### ORCID

Donghui Zhang: 0000-0003-0779-6438  
Vijay T. John: 0000-0001-5426-7585

### Notes

The authors declare no competing financial interest.

## ■ ACKNOWLEDGMENTS

We acknowledge Tianyi Yu (LSU) for assistance with materials characterization through NMR and melting-point determination. This work was supported by the U.S. Department of Energy under EPSCoR grant no. DE-SC0012432. The Research at Oak Ridge National Laboratory's Spallation Neutron Source was sponsored by the Scientific User Facilities Division, Office of Basic Energy Sciences, U.S. Department of Energy. We are grateful to Dr. William Heller (ORNL) for assistance with small-angle neutron scattering studies.

## REFERENCES

- (1) Peyman, G. A.; Ganiban, G. J. Delivery Systems for Intraocular Routes. *Adv. Drug Delivery Rev.* **1995**, *16*, 107–123.
- (2) Dhule, S. S.; Penfornis, P.; He, J. B.; Harris, M. R.; Terry, T.; John, V.; Pochampally, R. The Combined Effect of Encapsulating Curcumin and C6 Ceramide in Liposomal Nanoparticles against Osteosarcoma. *Mol. Pharmaceutics* **2014**, *11*, 417–427.
- (3) Dhule, S. S.; Penfornis, P.; Frazier, T.; Walker, R.; Feldman, J.; Tan, G.; He, J. B.; Alb, A.; John, V.; Pochampally, R. Curcumin-loaded gamma-cyclodextrin liposomal nanoparticles as delivery vehicles for osteosarcoma. *Nanomedicine* **2012**, *8*, 440–451.
- (4) Khuller, G. K.; Kapur, M.; Sharma, S. Liposome technology for drug delivery against mycobacterial infections. *Curr. Pharm. Des.* **2004**, *10*, 3263–3274.
- (5) Allen, T. M.; Austin, G. A.; Chonn, A.; Lin, L.; Lee, K. C. Uptake of liposomes by cultured mouse bone marrow macrophages: influence of liposome composition and size. *Biochim. Biophys. Acta, Biomembr.* **1991**, *1061*, 56–64.
- (6) Ricchelli, F.; Jori, G.; Gobbo, S.; Tronchin, M. Liposomes as Models to Study the Distribution of Porphyrins in Cell Membranes. *Biochim. Biophys. Acta, Biomembr.* **1991**, *1065*, 42–48.
- (7) Yoshina-Ishii, C.; Chan, Y. H. M.; Johnson, J. M.; Kung, L. A.; Lenz, P.; Boxer, S. G. Diffusive Dynamics of Vesicles Tethered to a Fluid Supported Bilayer by Single Particle Tracking. *Langmuir* **2006**, *22*, 5682–5689.
- (8) Lunelli, L.; Pasquardini, L.; Pederzoli, C.; Vanzetti, L.; Anderle, M. Covalently anchored lipid structures on amine-enriched polystyrene. *Langmuir* **2005**, *21*, 8338–8343.
- (9) Cooper, M. A.; Hansson, A.; Lofas, S.; Williams, D. H. A vesicle capture sensor chip for kinetic analysis of interactions with membrane-bound receptors. *Anal. Biochem.* **2000**, *277*, 196–205.
- (10) Boukobza, E.; Sonnenfeld, A.; Haran, G. Immobilization in surface-tethered lipid vesicles as a new tool for single biomolecule spectroscopy. *J. Phys. Chem. B* **2001**, *105*, 12165–12170.
- (11) Christensen, S. M.; Stamou, D. Surface-based lipid vesicle reactor systems: fabrication and applications. *Soft Matter* **2007**, *3*, 828–836.
- (12) Lahasky, S. H.; Hu, X.; Zhang, D. Thermoresponsive Poly(alpha-peptoid)s: Tuning the Cloud Point Temperatures by Composition and Architecture. *ACS Macro Lett.* **2012**, *1*, 580–584.
- (13) Gangloff, N.; Ulbricht, J.; Lorson, T.; Schlaad, H.; Luxenhofer, R. Peptoids and Polypeptoids at the Frontier of Supra- and Macromolecular Engineering. *Chem. Rev.* **2016**, *116*, 1753–1802.
- (14) Sun, J.; Zuckermann, R. N. Peptoid Polymers: A Highly Designable Bioinspired Material. *ACS Nano* **2013**, *7*, 4715–4732.
- (15) Zhang, D.; Lahasky, S. H.; Guo, L.; Lee, C.-U.; Lavan, M. Polypeptoid Materials: Current Status and Future Perspectives. *Macromolecules* **2012**, *45*, 5833–5841.
- (16) Murnen, H. K.; Rosales, A. M.; Dobrynin, A. V.; Zuckermann, R. N.; Segalman, R. A. Persistence Length of Polyelectrolytes with Precisely Located Charges. *Soft Matter* **2013**, *9*, 90–98.
- (17) Rosales, A. M.; Murnen, H. K.; Kline, S. R.; Zuckermann, R. N.; Segalman, R. A. Determination of the persistence length of helical and non-helical polypeptoids in solution. *Soft Matter* **2012**, *8*, 3673–3680.
- (18) Miller, S. M.; Simon, R. J.; Ng, S.; Zuckermann, R. N.; Kerr, J. M.; Moos, W. H. Proteolytic Studies of Homologous Peptide and N-substituted Glycine Peptoid Oligomers. *Bioorg. Med. Chem. Lett.* **1994**, *4*, 2657–2662.
- (19) Xuan, S.; Lee, C.-U.; Chen, C.; Doyle, A. B.; Zhang, Y.; Guo, L.; John, V. T.; Hayes, D.; Zhang, D. Thermoreversible and Injectable ABC Polypeptoid Hydrogels: Controlling the Hydrogel Properties through Molecular Design. *Chem. Mater.* **2016**, *28*, 727–737.
- (20) Lu, L.; Lahasky, S. H.; Zhang, D.; Garino, J. C. Directed Growth of Polymer Nanorods Using Surface-Initiated Ring-Opening Polymerization of N-Allyl N-Carboxyanhydride. *ACS Appl. Mater. Interfaces* **2016**, *8*, 4014–4022.
- (21) Hörtz, C.; Birke, A.; Kaps, L.; Decker, S.; Wächtersbach, E.; Fischer, K.; Schuppan, D.; Barz, M.; Schmidt, M. Cylindrical Brush Polymers with Polysarcosine Side Chains: A Novel Biocompatible Carrier for Biomedical Applications. *Macromolecules* **2015**, *48*, 2074–2086.
- (22) Laschewsky, A. Molecular concepts, self-organisation and properties of polysoaps. *Polysoaps/Stabilizers/Nitrogen-15 NMR*; Springer: Berlin, 1995; pp 1–86.
- (23) Raffa, P.; Wever, D. A. Z.; Picchioni, F.; Broekhuis, A. A. Polymeric Surfactants: Synthesis, Properties, and Links to Applications. *Chem. Rev.* **2015**, *115*, 8504–8563.
- (24) Trent, A.; Marullo, R.; Lin, B.; Black, M.; Tirrell, M. Structural properties of soluble peptide amphiphile micelles. *Soft Matter* **2011**, *7*, 9572–9582.
- (25) Douy, A.; Gallot, B. New amphipathic lipopeptides, 1. Synthesis and mesomorphic structures of lipopeptides with polysarcosine peptidic chains. *Makromol. Chem.* **1986**, *187*, 465–483.
- (26) Immordino, M. L.; Dosio, F.; Cattel, L. Stealth liposomes: review of the basic science, rationale, and clinical applications, existing and potential. *Int. J. Nanomed.* **2006**, *1*, 297–315.
- (27) Auguste, D. T.; Prud'homme, R. K.; Ahl, P. L.; Meers, P.; Kohn, J. Association of hydrophobically-modified poly(ethylene glycol) with fusogenic liposomes. *Biochim. Biophys. Acta, Biomembr.* **2003**, *1616*, 184–195.
- (28) Shen, W. W.; Boxer, S. G.; Knoll, W.; Frank, C. W. Polymer-Supported Lipid Bilayers on Benzophenone-Modified Substrates. *Biomacromolecules* **2001**, *2*, 70–79.
- (29) Chen, Y.; Javvaji, V.; MacIntire, I. C.; Raghavan, S. R. Gelation of Vesicles and Nanoparticles using Water-Soluble Hydrophobically Modified Chitosan. *Langmuir* **2013**, *29*, 15302–15308.
- (30) Shoji, Y.; Igarashi, T.; Nomura, H.; Eitoku, T.; Katayama, K. Liposome Solubilization Induced by Surfactant Molecules in a Microchip. *Anal. Sci.* **2012**, *28*, 339–343.
- (31) Lichtenberg, D.; Ahyauch, H.; Alonso, A.; Goñi, F. M. Detergent Solubilization of Lipid Bilayers: a Balance of Driving Forces. *Trends Biochem. Sci.* **2013**, *38*, 85–93.
- (32) Lichtenberg, D.; Ahyauch, H.; Goni, F. M. The Mechanism of Detergent Solubilization of Lipid Bilayers. *Biophys. J.* **2013**, *105*, 289–299.
- (33) Mattei, B.; França, A. D. C.; Riske, K. A. Solubilization of Binary Lipid Mixtures by the Detergent Triton X-100: The Role of Cholesterol. *Langmuir* **2015**, *31*, 378–386.
- (34) Lee, C.-U.; Smart, T. P.; Guo, L.; Epps, T. H.; Zhang, D. Synthesis and Characterization of Amphiphilic Cyclic Diblock Copolypeptoids from N-Heterocyclic Carbene-Mediated Zwitterionic Polymerization of N-Substituted N-carboxyanhydride. *Macromolecules* **2011**, *44*, 9574–9585.
- (35) Xuan, S.; Gupta, S.; Li, X.; Bleuel, M.; Schneider, G. J.; Zhang, D. Synthesis and Characterization of Well-defined PEGylated Polypeptoids as Protein-resistant Polymers. In Press. *Biomacromolecules* **2017**, DOI: 10.1021/acs.biomac.6b01824.
- (36) Holder, G. E.; McGary, C. M.; Johnson, E. M.; Zheng, R.; John, V. T.; Sugimoto, C.; Kuroda, M. J.; Kim, W.-K. Expression of the Mannose Receptor CD206 in HIV and SIV Encephalitis: A Phenotypic Switch of Brain Perivascular Macrophages with Virus Infection. *J. Neuroimmune Pharmacol.* **2014**, *9*, 716–726.
- (37) Liu, Y.; Li, M.; Yang, Y.; Xia, Y.; Nieh, M.-P. The Effects of Temperature, Salinity, Concentration and PEGylated Lipid on the Spontaneous Nanostructures of Bicellar Mixtures. *Biochim. Biophys. Acta, Biomembr.* **2014**, *1838*, 1871–1880.
- (38) Lee, J.-H.; Gustin, J. P.; Chen, T.; Payne, G. F.; Raghavan, S. R. Vesicle–Biopolymer Gels: Networks of Surfactant Vesicles Connected by Associating Biopolymers. *Langmuir* **2005**, *21*, 26–33.
- (39) Guinier, A.; Fournet, G. *Small Angle Scattering of X-rays*; John Wiley and Sons: New York, 1955.
- (40) Pabst, G.; Kučerka, N.; Nieh, M. P.; Katsaras, J. *Liposomes, Lipid Bilayers and Model Membranes: From Basic Research to Application*; CRC Press: Boca Raton, FL, 2014.
- (41) Lewis, B. A.; Engelman, D. M. Lipid bilayer thickness varies linearly with acyl chain length in fluid phosphatidylcholine vesicles. *J. Mol. Biol.* **1983**, *166*, 211–217.

(42) Balgavý, P.; Dubničková, M.; Kučerka, N.; Kiselev, M. A.; Yaradaikin, S. P.; Uhríková, D. Bilayer Thickness and Lipid Interface Area in Unilamellar Extruded 1,2-diacylphosphatidylcholine Liposomes: a Small-Angle Neutron Scattering Study. *Biochim. Biophys. Acta, Biomembr.* **2001**, *1512*, 40–52.

(43) Pedersen, J. S.; Schurtenberger, P. Scattering Functions of Semiflexible Polymers with and without Excluded Volume Effects. *Macromolecules* **1996**, *29*, 7602–7612.

(44) Chevrier, M.; Houston, J. E.; Kesters, J.; Van den Brande, N.; Terry, A. E.; Richeter, S.; Mehdi, A.; Coulembier, O.; Dubois, P.; Lazzaroni, R.; Van Mele, B.; Maes, W.; Evans, R. C.; Clement, S. Self-Assembled Conjugated Polyelectrolyte-Surfactant Complexes as Efficient Cathode Interlayer Materials for Bulk Heterojunction Organic Solar Cells. *J. Mater. Chem. A* **2015**, *3*, 23905–23916.

## Supporting Information

### **Amphiphilic Polypeptoids Serve as the Connective Glue to Transform Liposomes into Multilamellar Structures with Closely Spaced Bilayers**

Yueheng Zhang<sup>1</sup>, Sunting Xuan<sup>2</sup>, Olasehinde Owoseni<sup>1</sup>, Marzhana Omarova<sup>1</sup>, Xin Li<sup>3</sup>, Michelle E. Saito<sup>1</sup>, Jibao He<sup>4</sup>, Gary L. McPherson<sup>5</sup>, Srinivasa R. Raghavan<sup>6</sup>, Donghui Zhang<sup>2\*</sup> and Vijay T. John<sup>1\*</sup>

1. Department of Chemical and Biomolecular Engineering, Tulane University, New Orleans, LA 70118, United States
2. Department of Chemistry and Macromolecular Studies Group, Louisiana State University, Baton Rouge, LA 70803, United States
3. Louisiana Consortium for Neutron Scattering, Louisiana State University, Baton Rouge, LA 70803, United States
4. Coordinated Instrumentation Facility, Tulane University, New Orleans, LA 70118, United States
5. Department of Chemistry, Tulane University, New Orleans, LA 70118, United States
6. Department of Chemical and Biomolecular Engineering, University of Maryland, College Park, MD 20742, United States

\*Corresponding authors:

Vijay T. John, phone: 504-865-5883 e-mail: [vj@tulane.edu](mailto:vj@tulane.edu).

Donghui Zhang, phone: 225-578-4893 email: [dhzhang@lsu.edu](mailto:dhzhang@lsu.edu)

## S1 Synthesis of Monomers

### Melting Point Measurements of NCA Monomer

The melting points of NCA monomers were measured using Electrothermal Mel-Temp digital melting point apparatus. The sample was packed 3 mm high in a capillary tube and then heated in open air. The melting process was observed through the magnifying lens. The measurements were repeated four times to get the mean value and standard deviation. The melting point of *N*-decyl NCA is  $60.0 \pm 0.5$  °C ( $n=4$ ). *N*-methoxyethyl NCA is a liquid at room temperature, thus its melting point was not recorded.

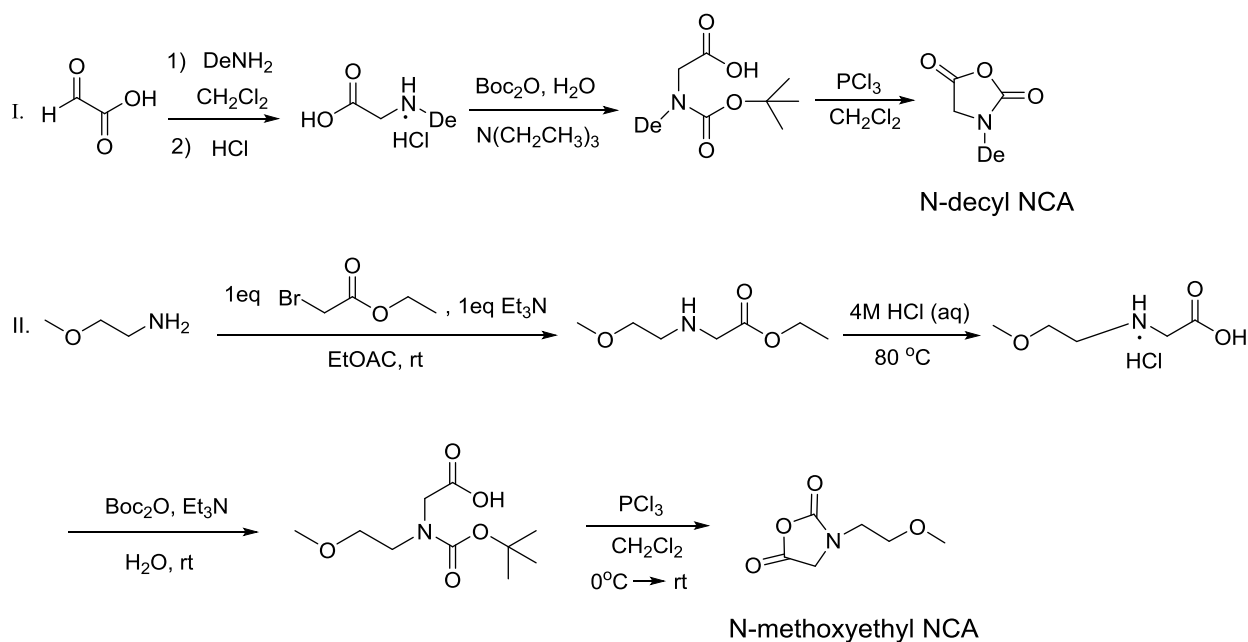
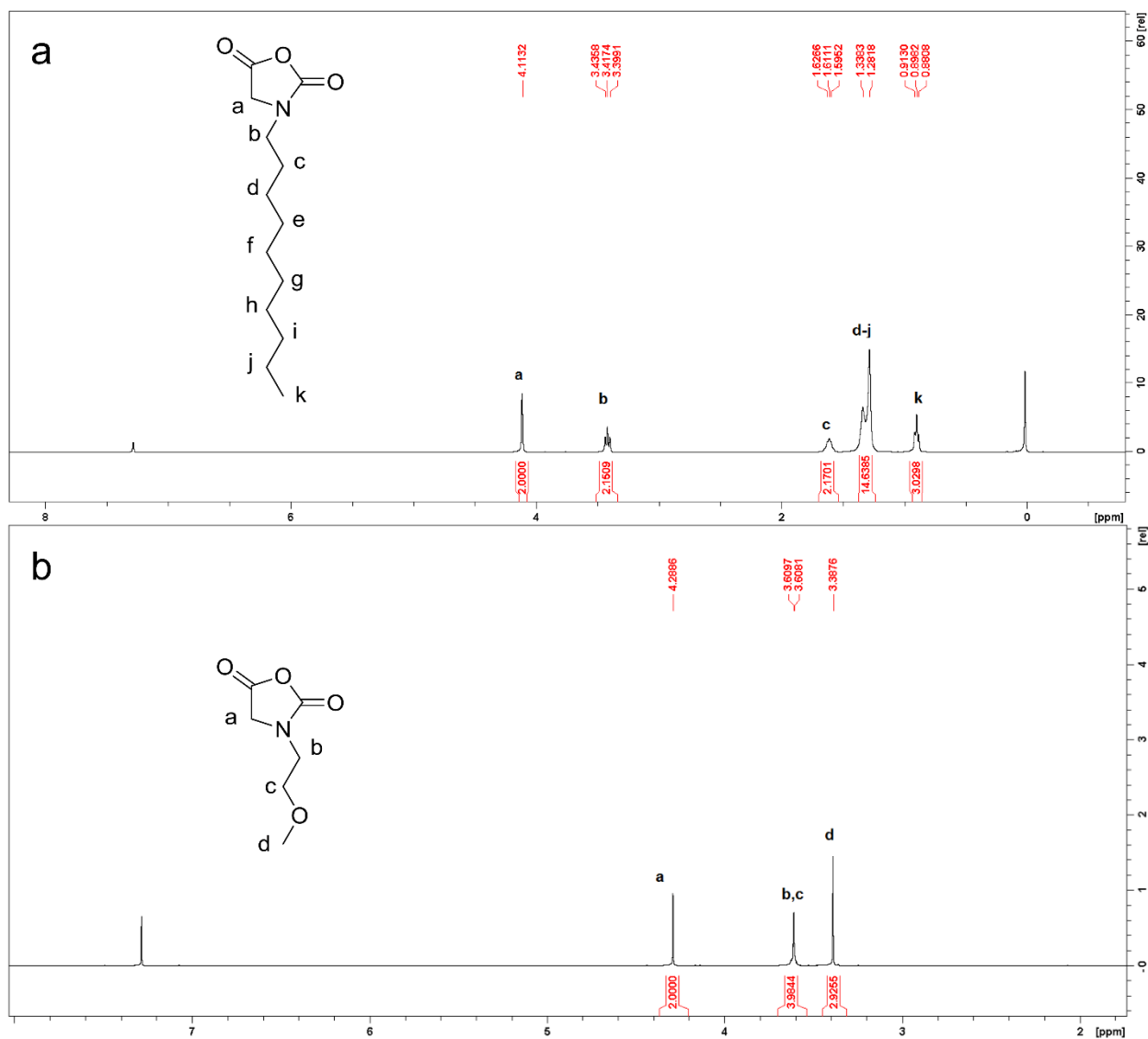


**Figure S1.** Synthesis routes of *N*-decyl NCA and *N*-methoxyethyl NCA monomers.



## S2 <sup>1</sup>H NMR of Monomers.

**Figure S2.** <sup>1</sup>H NMR of *N*-decyl NCA (a) and *N*-methoxyethyl NCA (b) in CDCl<sub>3</sub>.

*N*-decyl NCA <sup>1</sup>H NMR (400MHz, CDCl<sub>3</sub>) δ (ppm): 4.11 (s, -COCH<sub>2</sub>-), 3.44-3.40 (t, -NCH<sub>2</sub>-), 1.63-1.60(m, -NCH<sub>2</sub> CH<sub>2</sub>-), 1.34-1.28 (m, -NCH<sub>2</sub> CH<sub>2</sub> (CH<sub>2</sub>)<sub>7</sub> CH<sub>3</sub>) 0.91-0.88 (t, -CH<sub>3</sub>).

*N*-methoxyethyl NCA <sup>1</sup>H NMR (400MHz, CDCl<sub>3</sub>) δ (ppm): 4.29 (s, -COCH<sub>2</sub>-), 3.61(d, -NCH<sub>2</sub>CH<sub>2</sub>-), 3.39(s, -CH<sub>3</sub>)



### S3 $^{13}\text{C}\{^1\text{H}\}$ NMR of Monomers

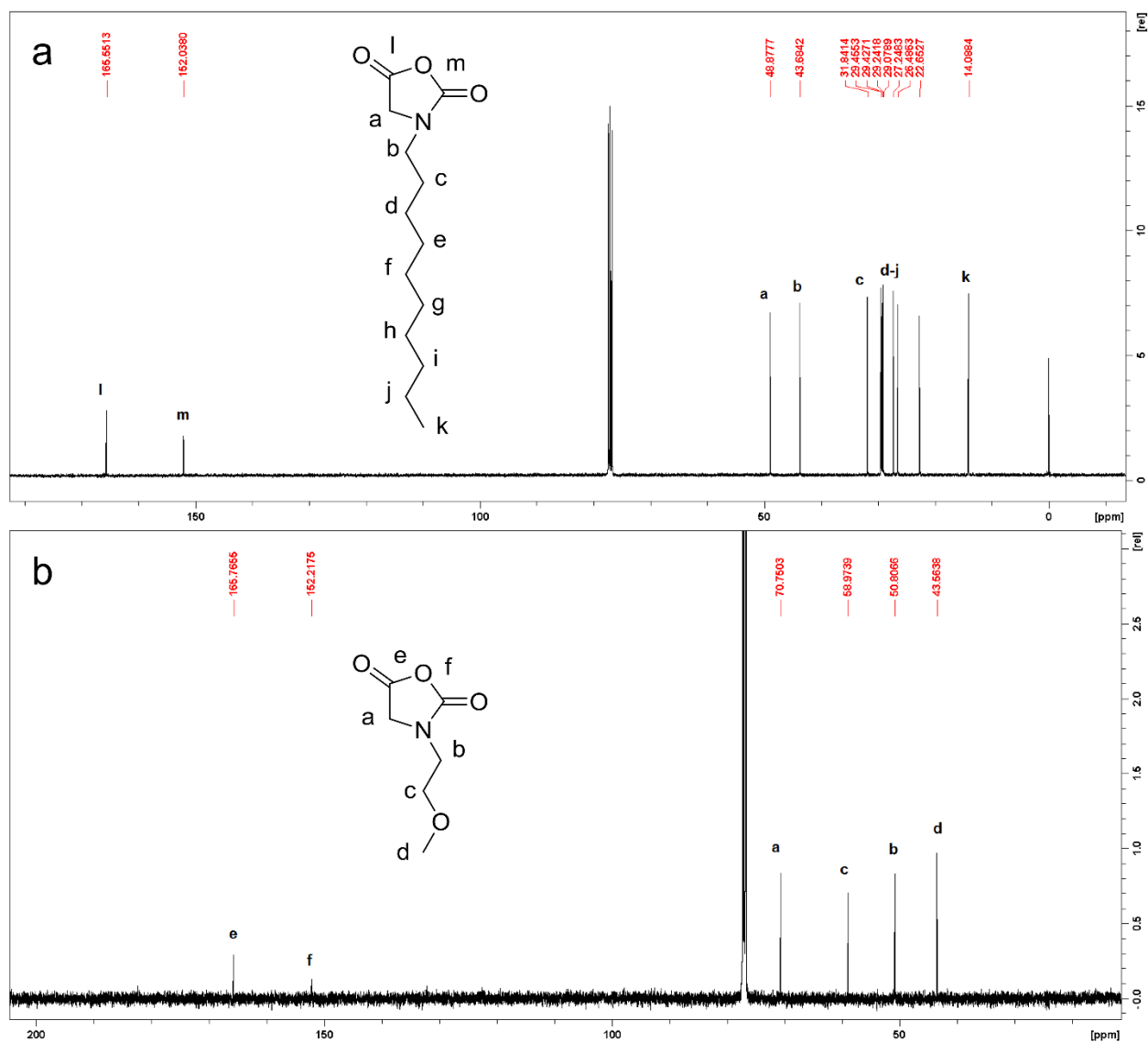


**Figure S3.**  $^{13}\text{C}\{^1\text{H}\}$  NMR of *N*-decyl NCA (a) and *N*-methoxyethyl NCA (b) in  $\text{CDCl}_3$ .

*N*-decyl NCA  $^{13}\text{C}\{^1\text{H}\}$  NMR (100MHz,  $\text{CDCl}_3$ )  $\delta$  (ppm): 165.6 ( $-\text{CH}_2\text{COO}-$ ), 152.0 ( $-\text{NCOO}-$ ), 48.9 ( $-\text{NCH}_2\text{CO}-$ ), 43.7 ( $-\text{NCH}_2\text{CH}_2-$ ), 31.8 ( $-\text{NCH}_2\text{CH}_2-$ ), 29.4-22.7 ( $-\text{NCH}_2\text{CH}_2(\text{CH}_2)_7\text{CH}_3$ ), 14.1 ( $-\text{CH}_3$ ).

*N*-methoxyethyl NCA  $^{13}\text{C}\{^1\text{H}\}$  NMR (100MHz,  $\text{CDCl}_3$ )  $\delta$  (ppm): 165.8 ( $-\text{CH}_2\text{COO}-$ ), 152.2 ( $-\text{NCOO}-$ ), 70.8 ( $-\text{NCH}_2\text{CO}-$ ), 59.0 ( $-\text{NCH}_2\text{CH}_2-$ ), 50.8 ( $-\text{NCH}_2\text{CH}_2-$ ), 43.6 ( $-\text{CH}_2\text{OCH}_3$ ).

## S4. $^1\text{H}$ NMR of Polypeptoids

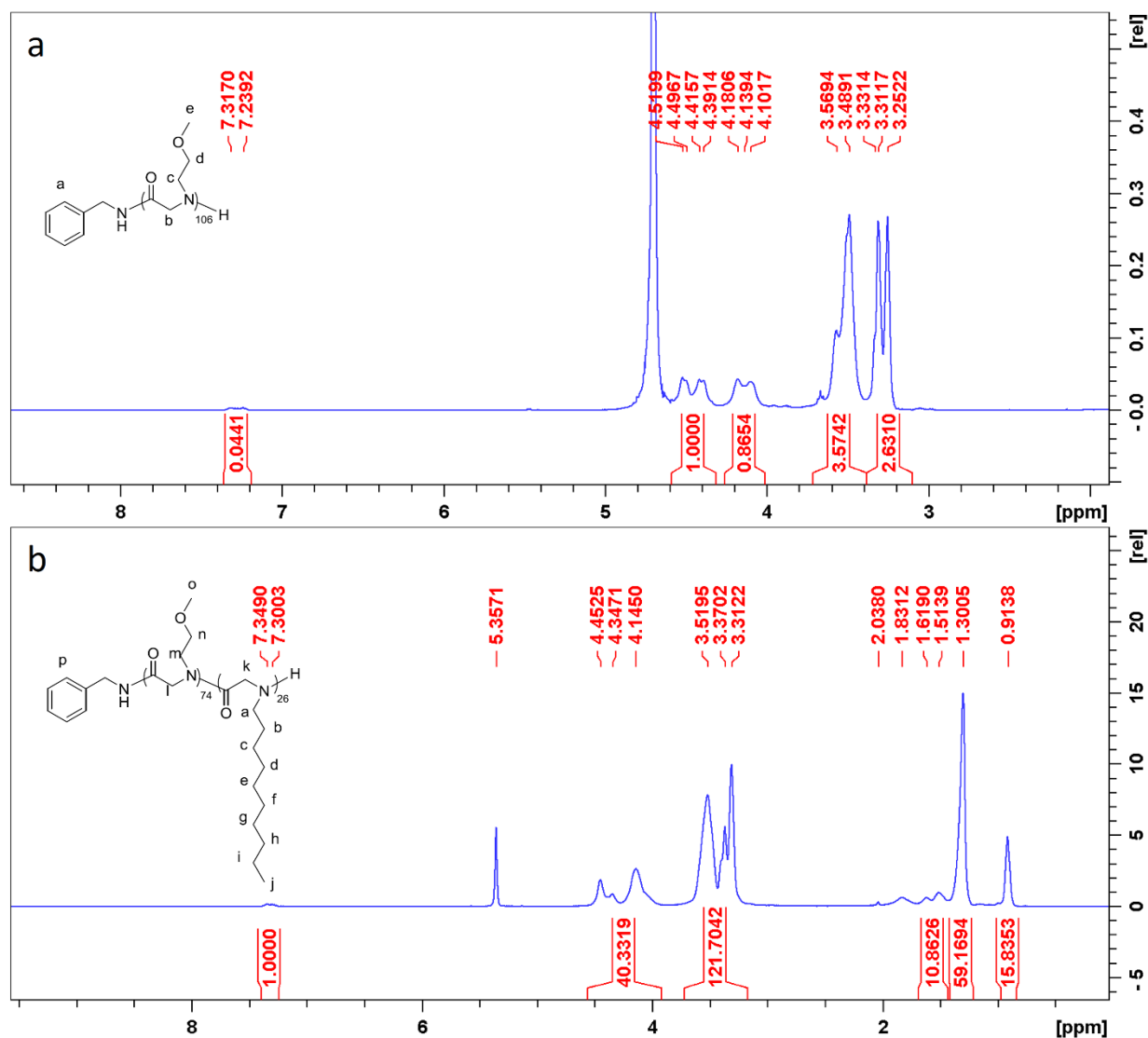


**Figure S4.**  $^1\text{H}$  NMR of UMP in  $\text{D}_2\text{O}$  (a) and HMP in  $\text{CD}_2\text{Cl}_2$  (b).

UMP  $^1\text{H}$  NMR ( $\text{D}_2\text{O}$ , 400 MHz)  $\delta$  (ppm): 7.31–7.24 (m,  $\text{C}_6\text{H}_5^-$ ), 4.10–4.52 (m,  $-\text{COCH}_2^-$ ), 3.49–3.57 (m,  $-\text{CH}_2\text{CH}_2\text{O}-$ ), 3.25–3.33 (m,  $-\text{OCH}_3$ ). HMP  $^1\text{H}$  NMR ( $\text{CD}_2\text{Cl}_2$ , 400 MHz)  $\delta$  (ppm): 7.30–7.34 (m,  $\text{C}_6\text{H}_5^-$ , 5H), 4.15–4.45 (m,  $-\text{COCH}_2^-$ ), 3.31–3.52 (m,  $-\text{CH}_2\text{CH}_2\text{OCH}_3$ ,  $-\text{NCH}_2^-$  (NDG)), 1.51–1.62 (m,  $-\text{NCH}_2\text{CH}_2^-$ , NDG), 1.30 (m,  $-\text{NCH}_2\text{CH}_2(\text{CH}_2)_6\text{CH}_2^-$ , NDG), 0.91 (s,  $-\text{CH}_3$ , NDG).

## S5. Size Exclusion Chromatography (SEC) of Polypeptoids

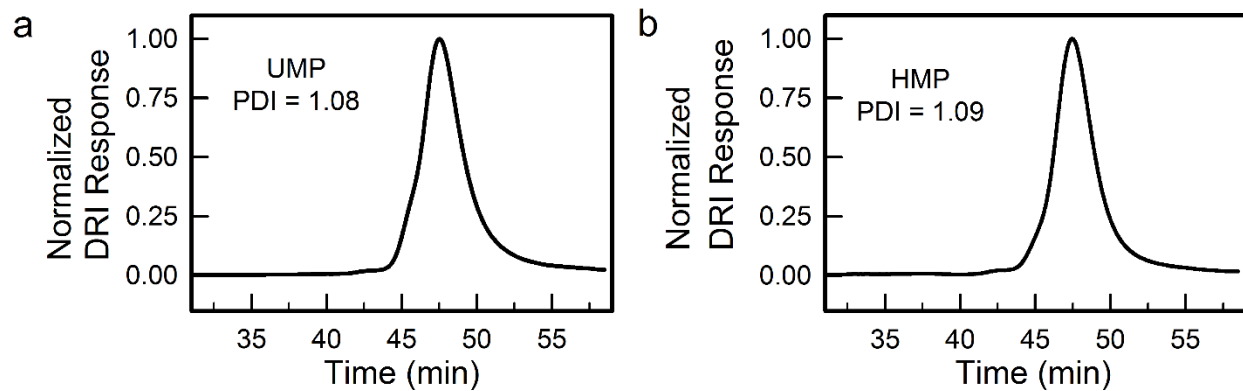


**Figure S5.** SEC chromatograms of UMP (a) and HMP (b) using polystyrene as the standard in LiBr/DMF (0.1M).

## S6. SANS Profiles of Polypeptoids and Lipid Mixtures at Low Q Range

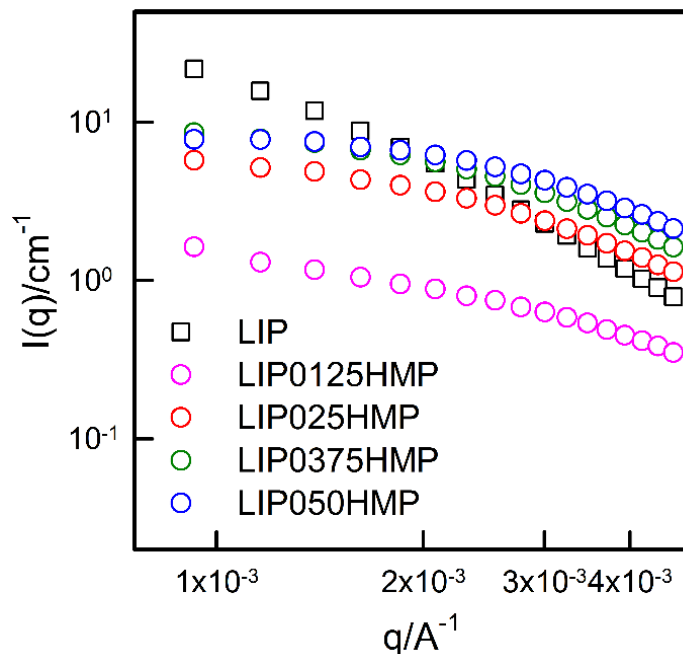
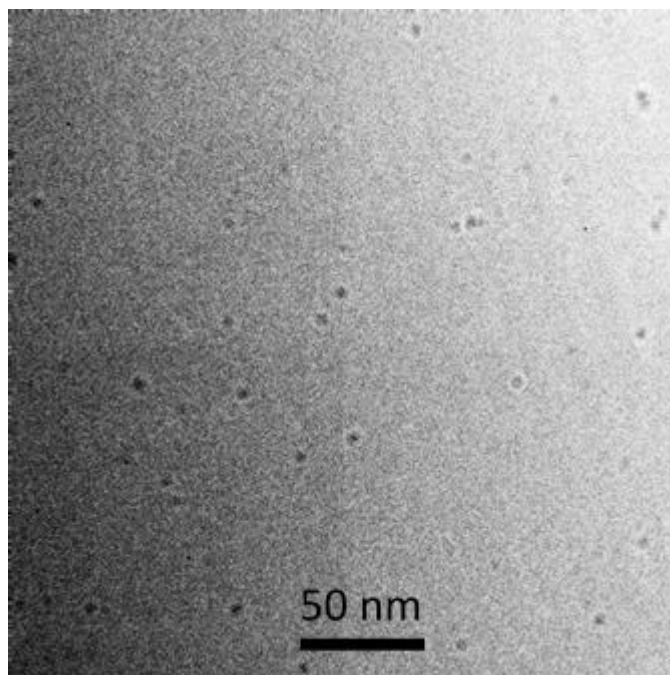


**Figure S6.** Unscaled low  $q$  range SANS data of 0.25% liposomes incubated with 0% HMP (LIP), 0.125% HMP (LIP0125HMP), 0.25% HMP (LIP025HMP), 0.375% HMP (LIP0375HMP) and 0.5% HMP (LIP050HMP). When HMP is added, the scattering intensity decreases dramatically.

Upon HMP addition, for each sample we observe a significant decrease in intensity at low  $q$ , compared to the control liposome sample (LIP). This indicates that HMP induces structural changes in the liposome structure.



**S7. Cryo-TEM Image of Lipid-HMP Thin Film Hydrated by DI Water**

**Figure S7.** Cryo-TEM image of lipid-HMP thin film hydrated by DI water.

We incorporated HMP in the plated out lipid system by dissolving all the components in a chloroform + methanol solution. Upon hydration there is no evidence of liposome formation in cryo-TEM images.